Acta Materialia 201 (2020) 494–503

Contents lists available at ScienceDirect

Acta Materialia

journal homepage: www.elsevier.com/locate/actamat

Point defects and interstitial climb of 90° partial dislocations in brown type IIa natural diamond

F.H.J. Laidlaw[a], R. Beanland[a,*], D. Fisher[b], P.L. Diggle[b]

[a] Department of Physics, University of Warwick, Coventry CV4 7AL, UK
[b] De Beers Group Technology, Maidenhead, SL6 6JW, UK

ARTICLE INFO

Article history:
Received 30 April 2020
Revised 25 August 2020
Accepted 16 October 2020
Available online 21 October 2020

Keywords:
Brown diamond
Faulted dipoles
Interstitial condensation
Stacking fault energy

ABSTRACT

Multiple electron microscopy techniques have been used to study a brown type IIa natural diamond. Electron backscatter diffraction shows evidence of plastic deformation in the form of slip bands, while cathodoluminescence reveals a network of low-angle grain boundaries, also observed in transmission electron microscopy together with long straight dislocations and dislocation dipoles. Aberration-corrected scanning transmission electron microscopy shows interstitial absorption on the 90° partial of both dissociated dislocations and Z-type faulted vacancy dipoles, forming structures similar to that observed in other fcc materials. The observations indicate an interstitial concentration of 10^{17} to 10^{19} cm^{-3} and calculations of point defect concentrations produced by plastic deformation show that this can be produced by strains of the order of 1%. Brown coloration in diamond has been previously attributed to vacancies and vacancy clusters with concentrations around 10^{18} cm^{-3}, which suggests that roughly equal numbers of interstitials and vacancies are generated in diamond via plastic deformation. Atomic resolution images of Z-type faulted dipoles allowed a stacking fault energy of 472 ± 38 mJ m^{-2} to be determined.

1. Introduction

Diamond has the interesting property that plastic deformation can produce brown coloration, an effect which is seen in natural stones of all types [1,2] as well as man-made crystals [3]. It can be seen as 'graining', i.e. brownish lines consistent with {111} slip bands [4]. Current consensus is that this coloration is caused by agglomerations of vacancies that are the result of plastic deformation. Supporting evidence for this theory includes positron annihilation spectroscopy (PAS), which indicates the presence of monovacancies and vacancy clusters in brown diamond (with concentrations ~10^{18} cm^{-3} or more [5,6]), absent in colourless stones. Modelling indicates that clusters of 30–60 vacancies have absorption spectra that would produce brown coloration [7,8]. Furthermore, high-pressure high-temperature (HPHT) treatment removes the brown colour [1,4,9,10] consistent with the dissolution of vacancy clusters. The possibility that dislocations are directly responsible for brown coloration can be discounted because, although there are many dislocations in natural brown diamond, HPHT treatment has no appreciable effect on their density [11]. Further evidence against dislocations being the direct cause of coloration is the observation that, while all brown diamonds have suffered plastic deformation, not all diamonds that are plastically deformed become brown [4,12]. (In fact this observation supports the hypothesis that point defects are responsible, as shown in Section 1.1 below.) Together, these observations imply that vacancy clusters form throughout the crystal by condensation from a supersaturation of point defects, while their removal by HPHT treatment presumably takes place by evaporation of vacancies from the cluster and their subsequent absorption by point defect sinks – or growth of clusters to become substantial voids with different absorption characteristics. It should be expected that both vacancies and self-interstitials are generated during plastic deformation, however little is discussed about the self-interstitials in the literature with relation to plastic deformation and the brown coloration in diamond.

In this article, the relationship between plastic deformation and point defects in a type IIa natural diamond with brown coloration is considered. Type IIa stones are studied due to their elemental purity, with a low nitrogen content (< 1 ppm), removing any confounding factors that could result from point defects generated by or reacting with nitrogen [13]. In particular, it removes the possibility that interstitials have been incorporated into platelets, an important by-product of the aggregation of nitrogen in type I diamonds. Our experimental observations primarily use electron microscopy, including atomic resolution scanning transmission elec-

* Corresponding author.
E-mail address: r.beanland@warwick.ac.uk (R. Beanland).

https://doi.org/10.1016/j.actamat.2020.10.033
1359-6454/

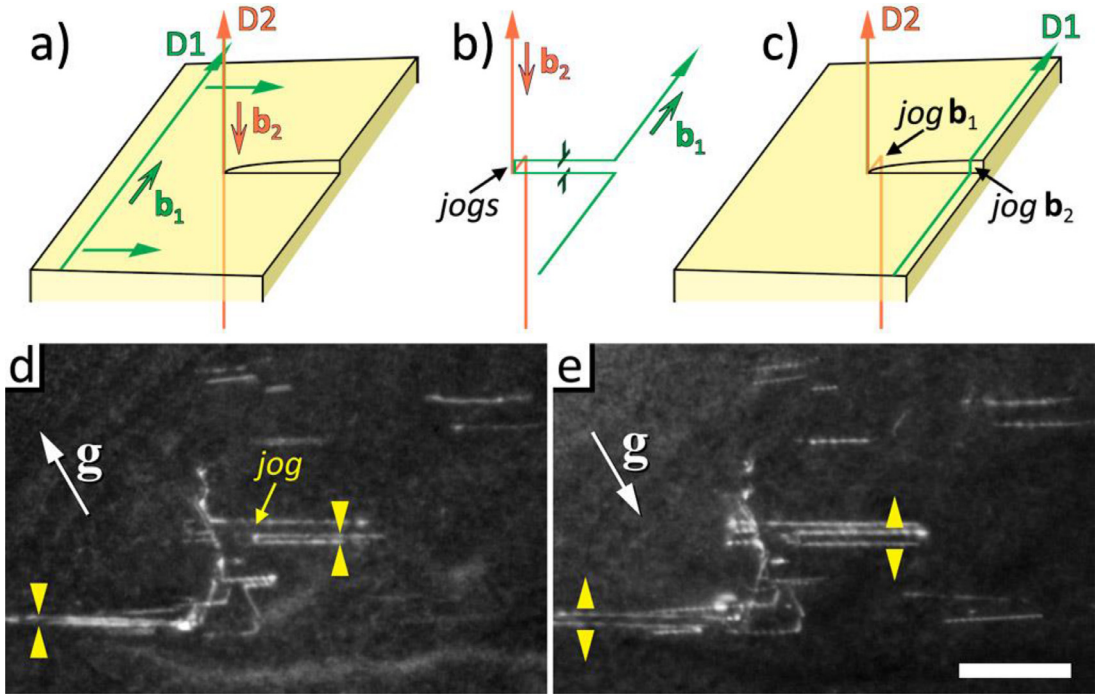

Fig. 1. Emission of point defects due to intersecting dislocations during plastic deformation. a) Dislocation D1 (green) lies in screw orientation with Burgers vector $\mathbf{b}_1$ and glides to the right on the plane shown, approaching dislocation D2 (orange), which cuts through the glide plane and has a screw component perpendicular to it $\mathbf{b}_2$. b) Once D1 passes through D2, both dislocations have a sessile jog, each with a size corresponding to the screw component of the Burgers vector of the other dislocation. As D1 moves to the right a dipole forms, anchored by the jog. c) the dipole in D1 can shrink by movement of the jog, in this case by emission of vacancies. After Amelinckx [17]. d) and e) dark field weak beam g3g = 220 TEM images of a dislocation dipole ending at a jog in a natural type IIa diamond with slight brown coloration. The bright line is displaced from the actual position of the dislocation, depending upon the local bending of the diffracting planes close to the dislocation core. The change in apparent separation of the pair of dislocations as g is reversed, indicated by the yellow arrowheads, indicate that they form a dipole [21]. Scale bar 100 nm. (For interpretation of the references to colour in this figure legend, the reader is referred to the web version of this article.)

tron microscopy (STEM), to study the dislocation microstructure. Previous attempts to directly observe vacancy clusters in brown diamond using high resolution STEM [14,15] have had limited success, since this technique is not particularly sensitive to the absence of a few atoms which might form a vacancy cluster. We also do not observe vacancy clusters. However, we are able to examine the core structure of dislocations. In the bulk of a pure crystal these are sinks for point defects, and therefore can give insight into the processes that have occurred. We find clear evidence that high concentrations of self-interstitials have condensed onto dislocations. These interstitial accretions are invisible in conventional weak-beam TEM and provide unequivocal evidence that self-interstitials are indeed generated by plastic deformation in fcc materials. We discuss our results with reference to previous observations in fcc materials (including both metals, and semiconductors with the diamond or zinc-blende structure). As a secondary aspect of our observations we use the atomic resolution images of faulted dipoles to calculate the stacking fault energy of diamond using the method of Steeds [16]. Before discussing the results, an introduction into the generation of point defects by plastic deformation and the intrinsic point defect behaviour of diamond is warranted.

1.1. Point defect generation by plastic deformation

The mechanism of point defect emission during plastic deformation in any material is shown in Fig. 1, following Amelinckx [17]. Two screw dislocations D1 and D2 are shown, with Burgers vector $\mathbf{b}_1$ and $\mathbf{b}_2$ respectively. D1 moves to the right on its glide plane, approaching D2 (Fig. 1a) and then passing through it (Fig. 1b). In doing so a jog is introduced in both dislocations; a jog of size $\mathbf{b}_1$ is produced in D2, and one of size $\mathbf{b}_2$ is produced in D1. These jogs can be sessile, in which case they can only move by emission or absorption of point defects. In Fig. 1b the jog in D1 acts as an anchor, and as D1 moves onwards it must leave behind a dipole, since the upper and lower arms attached to the jog now lie on parallel glide planes separated by $\mathbf{b}_2$ and cannot meet by glide. The attractive force between these two arms is of course huge, since they have opposite signs and are separated by a single lattice translation. It is energetically favourable for them to recombine and in doing so, emit point defects. Fig. 1c shows the final situation where the dipole has 'evaporated' by emission of point defects, in this case vacancies; the dipole in Fig. 1b is a vacancy dipole. Dissociation of dislocations into partials [18] does not change the total Burgers vector – or the size of the jog produced – when one dislocation passes through another. Interstitials are emitted by similar configurations with reversed Burgers vector or line direction of one of the dislocations, which produce interstitial dipoles. Since we may expect a variety of Burgers vectors in a deformed crystal, it therefore seems inevitable that both vacancies and interstitials are produced in plastic deformation, i.e. the type of point defect is determined primarily by geometry [19,20].

In fcc diamond, Burgers vectors of crystal dislocations are ½<110> type. The Burgers vector $\mathbf{b}_1$ must lie in a {111} glide plane, and $\mathbf{b}_2$ must have a component perpendicular to this {111} plane in order to produce a jog. Since half of all Burgers vectors lie in any given {111} glide plane this means that half of all possible interactions produce jogs in the fcc structure. Any two such dislocations always have a shared {111} glide plane that is different to the original one (with normal parallel to $\mathbf{b}_2 \times \mathbf{b}_1$). The jog can move conservatively, without emitting point defects, along the ⟨110⟩ direction that is the intersection of these two {111} planes. Conversely, perpendicular to this ⟨110⟩ direction, point defects must be produced to move D1 by a lattice translation vector. (In a simple fcc

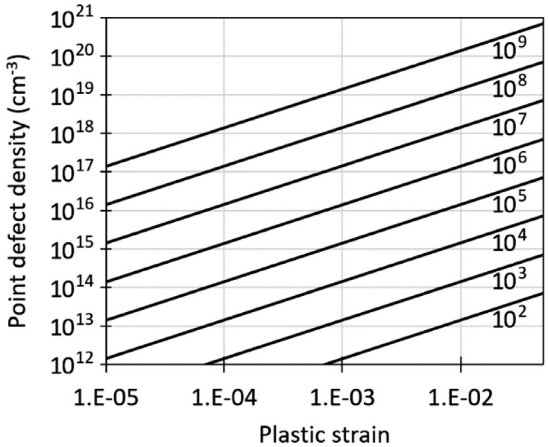

Fig. 2. Point defect concentrations generated during plastic deformation of diamond from Eq. (4). Each line corresponds to a different forest dislocation density, from 10^2 cm^{-2} to 10^9 cm^{-2}.

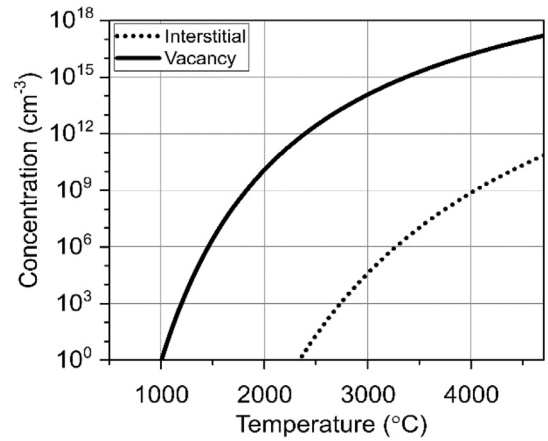

Fig. 3. Equilibrium concentration of interstitials and vacancies in diamond, from Eq. (1).

crystal this would be a single point defect; in diamond it is two.) The number of point defects emitted N is [17,22]

$$N = \frac{\hat{\mathbf{v}} \cdot (\mathbf{u}_2 \times \mathbf{u}_1)}{\left|\hat{\mathbf{v}} \cdot (\mathbf{u}_2 \times \mathbf{u}_1)\right|}\left[\hat{\mathbf{v}} \cdot (\mathbf{b}_2 \times \mathbf{b}_1)\right]\frac{L}{8a} \tag{1}$$

Where $\hat{\mathbf{v}}$ is a unit vector along the direction of motion for D1, L is the distance D1 has travelled from the intersection, a is the lattice parameter, and $\mathbf{u}_1$, $\mathbf{u}_2$ are the dislocation line directions (following the finish-start/right-hand (FS/RH) convention).

Importantly, the density of point defects produced by deformation is not only related to the plastic strain that the crystal experiences. The key point is that the active slip system must pass through a 'forest' of pre-existing dislocations that cut through the glide plane [23,24]. The dislocation D2 in Fig. 2 is such a forest dislocation, obstructing the slip of D1. The dislocations running vertically in Figs. 2d and 2e could also be forest dislocations. The number of point defects generated depends upon both the density of forest dislocations and the strain produced by the dislocations passing through them. This may explain why some diamonds that have been plastically deformed have no brown coloration; only crystals that experience deformation by more than one slip system will produce jogs by the mechanism shown in Fig. 1 and contain high point defect densities. Indeed, brown coloration is stronger in synthetic diamond deformed such that multiple slip systems operate simultaneously [3].

The total length of dragged jogs per unit volume λ, when a glissile array of dislocations producing plastic strain ε passes through an array of forest dislocations with density ρ is

$$\lambda = \frac{\rho\varepsilon}{4b}, \tag{2}$$

taking into account that half of the interactions produce no jogs. The concentration of point defects per unit volume produced by plastic strain is therefore

$$C = \frac{\hat{\mathbf{v}} \cdot (\mathbf{u}_2 \times \mathbf{u}_1)}{\left|\hat{\mathbf{v}} \cdot (\mathbf{u}_2 \times \mathbf{u}_1)\right|}\left[\hat{\mathbf{v}} \cdot (\mathbf{b}_2 \times \mathbf{b}_1)\right]\frac{\rho\varepsilon}{32ab}, \tag{3}$$

which is shown in Fig. 2 for different forest dislocation densities. A forest dislocation density of 10^9 cm^{-2} and a plastic strain of 1% can generate ~10^{20} point defects cm^{-3}.

Although this calculation predicts point defect concentrations significantly larger than the vacancy concentrations of 10^{18} cm^{-3} measured by PAS in brown diamonds, [5] the value given by Eq. (3) is almost certainly an overestimate. This is because a dislocation gliding through the crystal during plastic deformation may meet bundles of forest dislocations as well as single defects. If D2 is replaced in Fig. 2 by several forest dislocations that are too close together to allow the dislocation to pass between them, [24] the jog produced in D1 will be larger. The height of the dipole in Fig. 2b will be correspondingly larger and the driving force for recombination is reduced. Beyond a certain height the attractive force will not be sufficiently high to cause annihilation of the dipole, point defects will not be generated, and the dipole will remain stable. A good fraction – perhaps the majority – of jogs created by forest interactions may therefore not produce point defects since the dipoles they produce are too widely spaced. Indeed, dislocation dipoles are commonly observed in deformed fcc materials, [23,25-27] and chains of dislocation loops condensed from point defects produced by dipole collapse have also been observed [28]. We have not observed the latter, but an example of a dipole terminated by a jog in our brown type IIa diamond is shown in the dark field weak-beam (DFWB) TEM images Figs. 1d and 1e. Dislocation dipoles are apparent from the change in the apparent spacing of their constituent dislocations when the diffraction vector is reversed, [21] as shown by the yellow arrowheads. The jog is dissociated, with a faint loop visible to the left of the arrow.

1.2. Point defects in diamond

At finite temperatures, point defects p have an equilibrium concentration c_p that can be estimated by an Arrhenius law of the form [29]

$$c_p = n_p \exp(E_p^f / k_B T), \tag{4}$$

where n_p is the density of possible point defect p sites per unit cell, E_p^f is the formation energy of p, k_B is Boltzmann's constant and T is absolute temperature. In general, the formation energy of interstitials (E_i^f) is larger that of vacancies (E_v^f). In diamond $E_i^f \approx$ 12 eV, while for vacancies $E_v^f \approx$ 6 to 7 eV [30-34]. These large formation energies mean that the equilibrium point defect density in diamond below ~1000 °C is effectively zero (Fig. 3). However, the formation energy is miniscule in comparison with that released by a moving dislocation in a stressed crystal and it can be appreciated by comparing Figs. 2 and 3 that large point defect supersaturations may easily be produced by plastic deformation.

Once point defects are formed, they may diffuse through the crystal lattice, which is also a thermally controlled process that follows an Arrhenius law. The behaviour of a point defect population far from equilibrium is determined primarily by the migration enthalpy E^m and at low temperatures, point defect diffusion may be 'frozen out'. In diamond, interstitial atoms have mi-

gration enthalpies of $E_i^m \approx 1.6$ eV and are only mobile at temperatures >330 °C, while vacancies begin to migrate significantly above ~570 °C with $E_v^m \approx 2.3$ eV [30-34]. Lithospheric diamonds may reside in the mantle for up to 10^9 years while experiencing temperatures in the range 900–1400 °C, [2,35] meaning that both vacancies and interstitials should be mobile when produced by plastic deformation and rapidly convert into stable clusters or be absorbed at other point defect sinks. In this work, the dislocation microstructure of a brown diamond is examined for evidence of these processes.

2. Experimental

The sample used in this study originated from a single natural type IIa diamond with a faint brown colour, which was cut and polished into a cube with {100} faces approximately 0.5 mm in size. The exact origin of the diamond is not known as it was selected from material aggregated from a number of productions, but is likely to be of southern African origin. It was left in an untreated state.

Electron backscatter diffraction (EBSD) mapping was performed on a FEI Versa at 20 kV with an Oxford Instruments Symmetry EBSD system. EBSD was carried out with the sample tilted at 70°, a working distance of 14.1 mm, step size of 3.1 µm and a probe current of 14µA. Cathodoluminescence (CL) imaging was carried out in a Zeiss Supra VP55 FEGSEM fitted with a Gatan MonoCL3 spectrometer at an accelerating voltage of 5 kV. Photoluminescence (PL) was carried out using a Horiba YobinYvon LabRam spectrometer equipped with a 660 nm excitation laser and Renishaw inVia confocal microscope equipped with a 325 nm HeCd laser. A JEOL 4500 focused ion beam (FIB) was used to cut lamellae parallel to {110} planes from selected sites using standard FIB preparation methods. Annular Dark Field Scanning Transmission Electron Microscopy (ADF-STEM) imaging was carried out using a JEOL ARM200F with double aberration correction at 200 kV. The beam convergence semi-angle was 22 mrad, giving a probe size ~0.75 nm at a beam current of 100 pA and the ADF detector covered an angle from 45 to 180 mrad. Multiple frames were taken with a fast scan (5μs/pixel) to limit beam damage and distortions due to drift.

3. Results

3.1. Spectroscopy and low-resolution microscopy

No single or aggregated forms of substitutional nitrogen were found in FTIR spectroscopy, confirming the type IIa nature of the diamond ([N] < 1 ppm). Photoluminescence (PL) spectroscopy (Fig. 4a) showed broad "band-A" luminescence centred at ~430 nm, known to be associated with dislocations and grain boundaries; [36-38] while the higher sensitivity of PL, compared to FTIR spectroscopy, also detected very small amounts of nitrogen-vacancy complexes H3 (N-V-N) and N3 (3N-V). A similarly small peak corresponding to the neutral vacancy centre, commonly referred to as the GR1 centre, was also detected.

Examination of the stone using optical microscopy, EBSD, and CL gave clear evidence of significant plastic deformation. Fig. 4b shows an optical image and Fig. 4c an EBSD map of crystal orientation on one of the {001} faces. Undulating strands of material with a similar orientation (misorientation < 2°), each several hundred microns wide, run across the whole of the face at an angle of 45°±10°, which is consistent with the intersection of a {111} glide system with the polished crystal surface. These features are similar to slip bands seen in heavily deformed fcc metals [27]. Strong band-A luminescence was observed by CL, and panchromatic images of the surface reveal a microstructure of sub-grain boundaries forming a cellular granular network over tens of micrometres (Fig. 4d), with a much lower density of dislocations (~ 1 × 10^8 cm^{-2}) between them (Fig. 4e). Sub-grain boundaries are often located at the edges of misorientation bands (see supplementary information Fig. S1). Band-A luminescence is strongest adjacent to sub-grain boundaries and decays over several microns, while material between has a specked appearance. The sub-grain boundaries themselves and individual dislocations appear dark, as expected for non-radiative recombination centres.

Cross section TEM lamellae taken parallel to {110} show the sub-grain boundaries to be inclined to the crystal surface, roughly on {111} planes (Fig. 4f, g). These sub-grain boundaries take the role of forest dislocations, through which cut long, straight individual dislocations and dipoles with <110> line directions that are the result of subsequent plastic deformation. Since the specimen is viewed in transmission, the atomic structure of line defects can only be discerned if they lie along the electron beam direction. Most of the individual defects in Fig. 4e lie along ⟨110⟩ directions at 60° to the plane of the lamella and are thus inaccessible, but a small number had line directions perpendicular to the section. These were examined using atomic resolution ADF-STEM, with the unexpected finding that all dislocations had absorbed interstitials, resulting in climb of a few atomic layers invisible to conventional diffraction contrast TEM.

3.2. Atomic resolution stem

Fig. 5a shows an ADF-STEM image of a typical 60° dislocation, viewed along a ⟨110⟩ direction. The Burgers vector component parallel to the beam direction cannot be determined, but for definiteness we assume that it has a component pointing into the image, i.e. the Burgers vector is $\boldsymbol{b} = \frac{1}{2}[01\bar{1}]$, with the line direction also pointing into the image according to the FS/RH convention [29]. The dislocation is dissociated and the schematic (Fig. 5d) shows the intrinsic stacking fault in green, bounded at its lower end by a 30° partial dislocation in red with $\boldsymbol{b} = \frac{1}{6}[\bar{1}2\bar{1}]$. The stacking fault is 2.40 nm wide. At the upper end of the stacking fault one would expect a 90° Shockley partial dislocation, with $\boldsymbol{b} = \frac{1}{6}[11\bar{2}]$. However, climb has occurred by the condensation of interstitial carbon atoms, moving the partial dislocation out of the glide plane towards the top right of the image by approx. six lattice translations, highlighted in dark blue in Fig. 5d. (Note that climb by absorption of vacancies would produce movement in the opposite direction, towards the bottom left. This was never observed.) This distinctive structure, i.e. a dissociated core and climb of only the 90° partial, was observed for all dislocations imaged. On close inspection of the climbed region in Fig. 5a it is apparent that the atom pairs ('dumbbells') cannot be distinguished in the climbed region, with rather blurred and indistinct atom columns, indicating that the structure varies along the electron beam path through the thin lamella. A measurement of the lattice displacement across the stacking fault is difficult because it is only a few atoms wide, and the material is distorted by the strain field of the dislocations. An estimate may be obtained using Fourier filtering to extract the $(11\bar{1})$ fringes (Fig. 5b), from which an intensity profile is taken along the line A-B (Fig. 5c). The lattice displacement can be obtained by comparing the actual profile (dark blue) with fringes extrapolated across the fault (light blue). The displacement in Fig. 5 is only 0.33 of a complete $(11\bar{1})$ plane spacing, consistent with the appearance of only single atoms rather than dumbbells in the climbed region. The component of the fault vector in the plane of the image is therefore $\frac{1}{9}[11\bar{1}]$. A second example is given in supplementary Fig. S2, with a displacement of 0.38 of a plane spacing.

Dislocation dipoles were also observed. These were all faulted vacancy Z-type dipoles and all showed climb of their 90° partials. Fig. 6 shows three examples. Each dipole consists of two 90° Shockley partial dislocations (partials 1 and 4, Fig. 6d), two $\frac{1}{6}$⟨110⟩

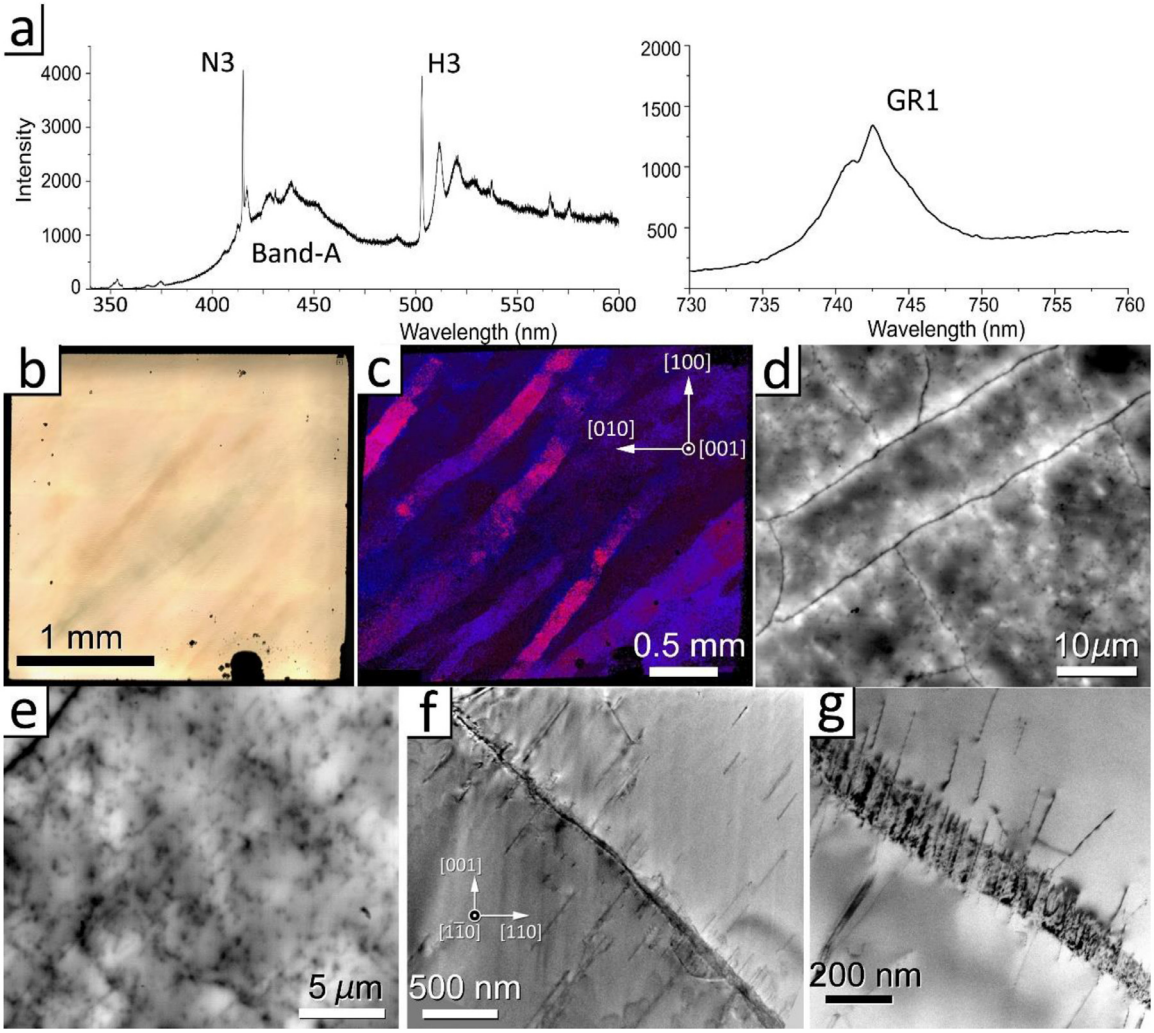

Fig. 4. Spectroscopy and microstructure of the untreated stone used in this study. a) PL spectra at 83 K showing band-A luminescence as well as H3, N3 and GR1 centres. b) Reflection optical image of the (001) surface showing the brown coloration in bands (edges of the image are parallel to {100}). c) EBSD orientation map of the same surface showing a banded structure. d) Room temperature panchromatic CL at 5 kV incident electron beam energy showing bright luminescence around sub-grain boundaries and patchy luminescence between; e) Panchromatic CL image (−168 °C) between the sub-grain boundaries showing dark spots corresponding to individual dislocations; f) Cross section TEM image of a sub-grain boundary and straight dislocations. Surface of the sample is towards the top of the image. g) The same boundary seen at an angle showing the high density of dislocations.

stair-rod dislocations (partials 2 and 3, Fig. 6d) and three intrinsic stacking faults [16,21,28,39-43]. The 90° climbed lengths vary from 5 to 9 lattice spacings. For the dipoles in Figs. 6a and 6b the displacement across the faults is about 0.4 of a {111} plane spacing, similar to that of individual dislocations. Interestingly, the amount of climb on both partials in a given dipole is the same, which implies that it is determined by the local interstitial concentration on a length scale much larger than the dipole height. For the dipole in Fig. 6c, with a greater amount of climb, complete dumbbells can be seen in the climbed section and the displacement is measured at 1.1 times a $(11\bar{1})$ plane spacing. (The displacement of slightly more than a complete plane spacing is due to the effect of the dislocation strain fields.) There also appears to be some climb of the upper stair-rod dislocation, with a slightly increased thickness of the intrinsic stacking fault.

An estimate of the concentration of interstitials absorbed onto the partials can be given by

$$C_{int} = R\rho n \tag{5}$$

Where R is the number of atoms required per unit length of dislocation line for the climb of one glide plane, ρ is the dislocation line density and n is the number of glide planes climbed. Dislocation climb in which just one interstitial atom is accommodated per periodic unit along the dislocation core requires $R \sim 4 \times 10^7$ atoms cm^{-1} of dislocation length. In this stone the dislocation density is ~10^9 cm^{-2} and climb of between five and twenty atoms has occurred, giving an absorbed interstitial concentration of 10^{17} to 10^{19} cm^{-3}.

3.3. Determination of the stacking fault energy

Atomic resolution ac-STEM images of the faulted dipoles allowed measurements of dissociation widths and dipole heights with much higher precision than is possible using conventional DFWB TEM images. The measured height and widths can be used to calculate stacking fault energy (SFE) by the equations described in SI3, assuming that an equilibrium configuration was attained before climb occurred. The equilibrium configuration is obtained when the mutually repulsive forces between the partial dislocations is balanced against the extension of the stacking fault, within the framework of anisotropic elasticity [16] (see SI3). The equilibrium configurations of the Z-type faulted dipole for different SFEs

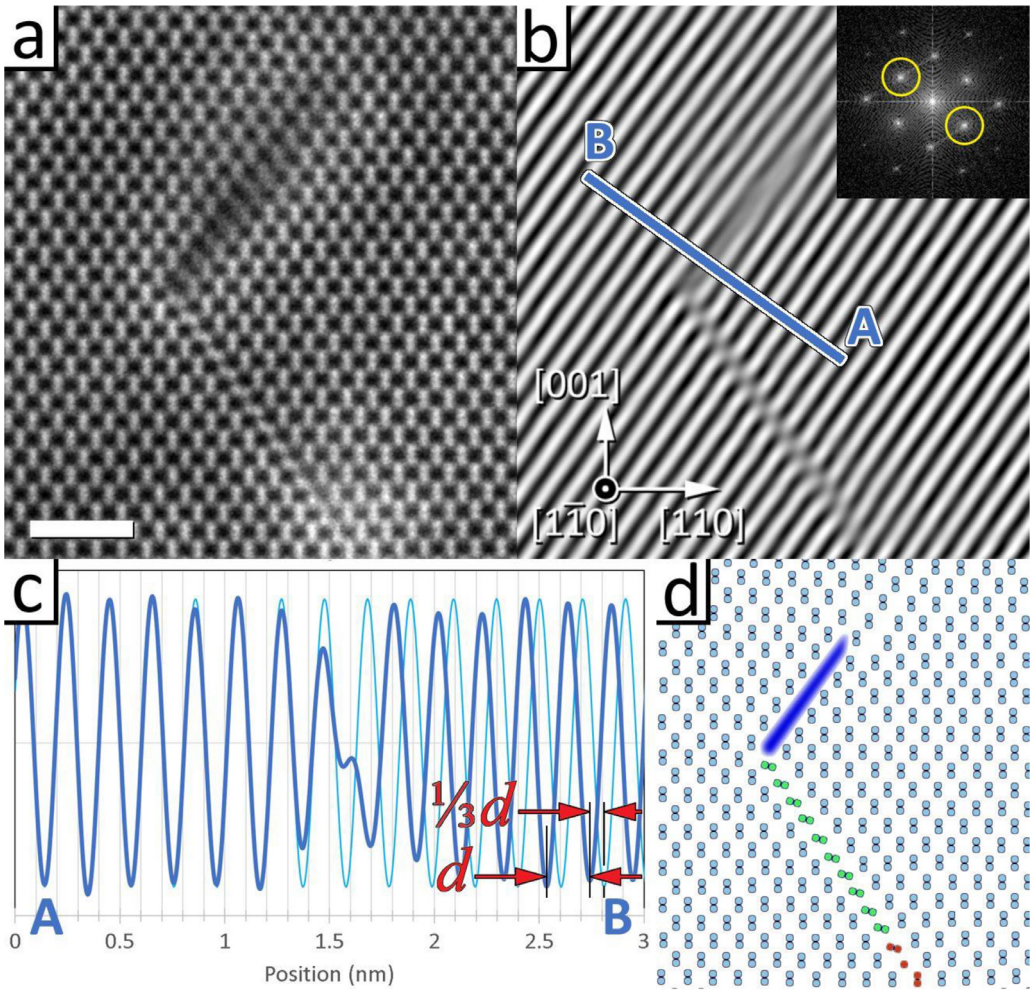

Fig. 5. a) ADF-STEM image of a dissociated ½[01$\bar{1}$] : (111) dislocation in an untreated brown diamond, in the vicinity of the low angle grain boundary shown in Fig. 3d, with a 90° partial that has climbed by addition of interstitial atoms over several lattice planes (scale bar 1 nm); b) Fourier filtered image showing the (11$\bar{1}$) planes (inset shows FFT and circular masks used); c) intensity plot along A-B (dark blue) and extrapolated period (light blue) showing that there is a shift of one third of the lattice period across the climbed fault; d) schematic of the defect highlighting the 30° partial dislocation with Burgers vector ⅙[$\bar{1}$2$\bar{1}$] (red) bounding an intrinsic stacking fault (green) and climbed 90° Shockley partial (dark blue). (For interpretation of the references to colour in this figure legend, the reader is referred to the web version of this article.)

has been plotted in Fig. 7, showing the separation between the 90° Shockley partial and the stair-rod dislocation as a function of dipole height, along with the measured values for the dipoles seen in Fig. 6. We obtain a SFE of 472 ± 38 mJ m^{-2}.

4. Discussion

The dislocation microstructure gives clear evidence that a high concentration of interstitials was produced at some point in the life of the Type IIa diamond studied here. Before discussing the results in detail, it is worth establishing that plastic deformation is the only mechanism that could be responsible. There are three alternative mechanisms. First, quenching to produce high point defect concentrations has been used in the past to produce similar climbed microstructures in Si, Ga and GaAs [45,46]. However, to achieve interstitial and vacancy concentrations > 10^{17}cm^{-3} requires quenching from extremely high temperatures, Fig. 1, > 4000 °C for vacancies and > 6000 °C for interstitials. There is no credible terrestrial mechanism that would provide a rapid quench from these temperatures.

A second method to create large point defect densities, often used in experimental studies, is through irradiation to produce Frenkel pairs [12,47]. In diamond this results in the presence of the GR1 (neutral vacancy centre) spectral feature and green coloration, [48] which can be turned into brown colouration by annealing. Natural irradiation of diamond in the mantle by alpha-decay radiogenic elements (^{232}Th, ^{235}U, ^{238}U) produces green coloration at the surface due to the small penetration depth of alpha particles [48,49]. In our study the stones were cut and polished into {100} facetted cubes removing any surface material that could have been irradiated. The main beta-decay element in the Earth's crust is ^{40}K, which can produce Frenkel pairs in a diamond's interior, but is very scarce in the Earth's mantle. The small GR1 peak shown in Fig. 4a is thus probably a result of examination by SEM and FIB prior to PL. While the accelerating voltage used for TEM and STEM (200 kV) is close to the damage threshold for [110] diamond (~220 kV), [50] no sample annealing was carried out at any point that would allow point defect migration [51] to the dislocations. Thus, neither natural radiation, nor the experimental methods used, could produce these structures.

Thirdly, aggregation of nitrogen in diamond can produce high supersaturations of interstitials during the formation of the *B*-centre, which consists of four nitrogen atoms surrounding a vacancy. The vacancy is produced by expulsion of a carbon atom once the four N atoms aggregate (typically at temperatures above 600 °C). Nitrogen concentrations of a few thousand ppm can be found in type I diamonds, [52] producing over 10^{20} cm^{-3} inter-

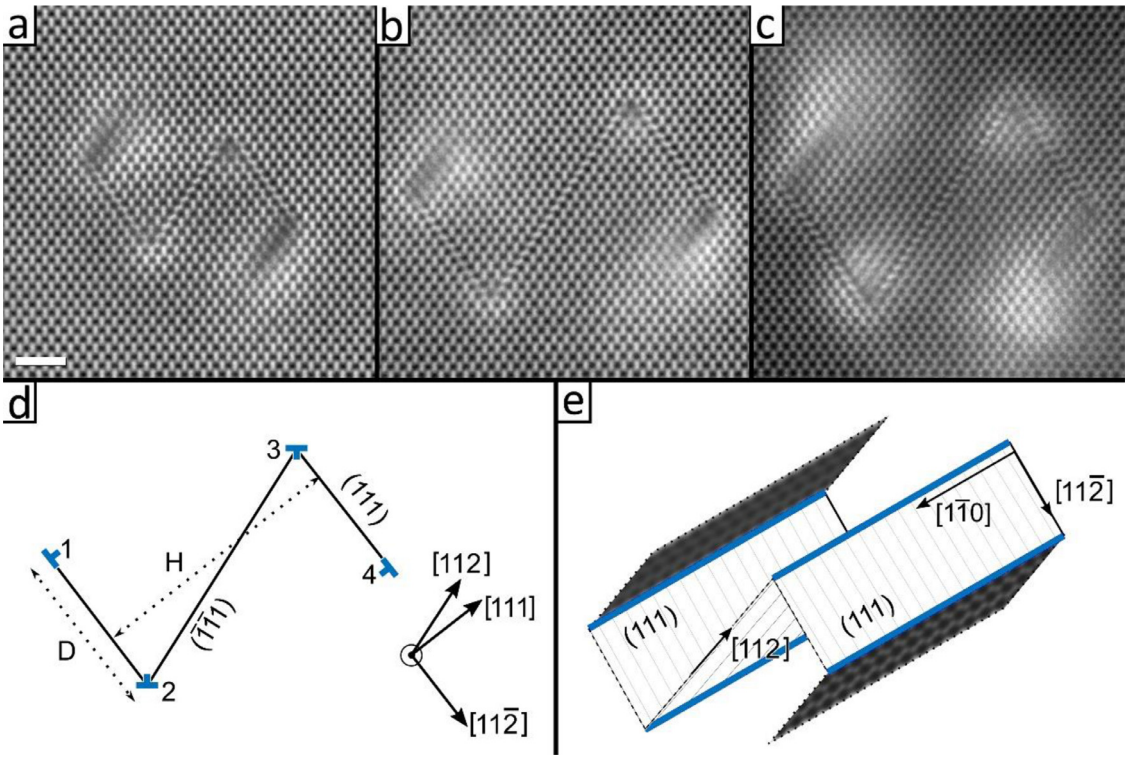

Fig. 6. (a), (b), (c) ADF-STEM images of faulted dislocation dipoles in an untreated brown diamond that have undergone climb through addition of interstitial atoms. (scale bars 1 nm) (d) Schematic of faulted dipole, 1) $\boldsymbol{b} = \frac{1}{6}[\bar{1}\bar{1}2]$, 2) $\boldsymbol{b} = \frac{1}{6}[\bar{1}\bar{1}0]$, 3) $\boldsymbol{b} = \frac{1}{6}[110]$, 4) $\boldsymbol{b} = \frac{1}{6}[11\bar{2}]$. Dislocations 1 and 4 are 90° partials. Dislocations 2 and 3 are stair rod partial dislocations. (e) 3D schematic showing interstitials condensed on the 90° partial dislocations of the faulted dipole. Stair-rod and 90° partial dislocations are highlighted in blue.(For interpretation of the references to colour in this figure legend, the reader is referred to the web version of this article.)

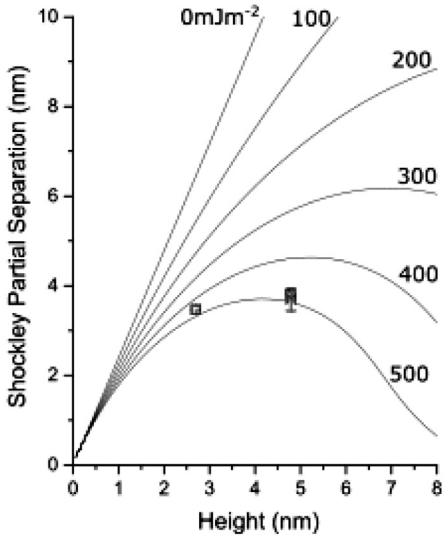

Fig. 7. Equilibrium Shockley partial separation vs dipole height for different values of stacking fault energy. Points mark the Shockley partial separation and heights of the dipoles in Fig. 6. Error bars represent a change in separation of 1 lattice spacing. Uncertainties in elastic constants are negligible (from [44], ~0.02% in c_{11}, c_{12} and c_{44}).

stitials, with the interstitials then condensing into the well-known platelets on {100} planes [53] (and from the evidence presented here, we might also expect them to produce dislocation climb). Platelets are almost exclusively seen in diamond containing aggregated forms of nitrogen [52]. The type IIa diamond examined here contains no *B*-centres and very low concentrations (< 1 ppm) of H3 and N3 nitrogen-vacancy complexes. Nitrogen aggregation cannot be the source of the interstitial concentration we observe.

We therefore estimate that 10^{17} to 10^{19} cm^{-3} interstitial atoms were generated by plastic deformation in the stone examined here. Previous PAS studies of similar brown type IIa diamonds gave vacancy concentrations of approx. 10^{18}cm^{-3} [1,5,8,12,54]. This close match strongly suggests that equal numbers of vacancies and interstitials are generated by plastic deformation, although their fates, once produced, are rather different.

Dislocation climb due to absorption of interstitial atoms has been observed previously in materials with diamond and zinc-blende structure, but not in diamond itself. The climbed 90° Shockley partial in Fig. 5a appears identical to those observed in silicon by Thibault-Desseaux et al. (TD) [45], who used high-resolution TEM to examine climb of many such dislocations in silicon deformed at high temperatures and cooled under load. Point defects in silicon, under the conditions used by TD, have an equilibrium concentration close to zero due to relatively high formation energies, [55] and are highly mobile (migration enthalpies of $E_v^m <$ 0.5 eV [56] and $E_i^m \approx$ 1.8 eV [57]). This is essentially the same deformation regime as diamond experiences in the mantle and it is pleasing to see similar microstructures in both materials. They interpreted their observations as the nucleation of a prismatic ½ [011] loop on the 90° $\frac{1}{6}[11\bar{2}]$ partial on an inclined {111} plane, as shown schematically in Fig. 8a, where Burgers vectors are given in Thomson tetrahedron notation [45,58,59]. Due to lack of resolution at the time they were unable to confirm the details of this model. In our higher resolution ADF-STEM images, a prismatic loop like that shown in Fig. 8a should appear as a full bilayer of additional atoms (a complete extra $(11\bar{1})$ plane) in the climbed fault. However, for most defects we do not observe a complete bilayer – only single atoms can be seen in the additional layer and the displacement across the fault is about 40% of a complete plane. Only in one case (Fig. 5c) do we observe a complete bilayer and a displacement of a complete plane. One interpretation of these

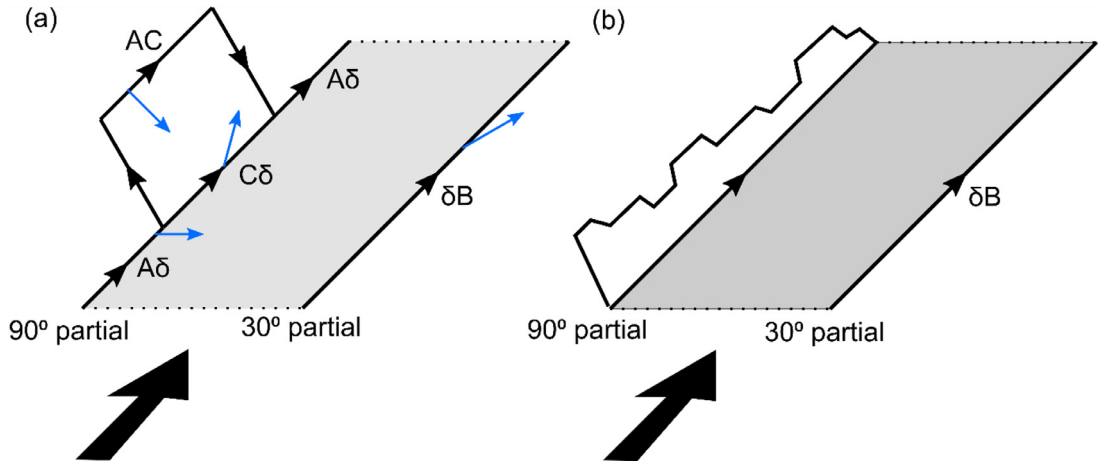

Fig. 8. (a) Dislocation climb by growth of a prismatic dislocation loop on the 90°partial dislocation, after [45]. Burgers vectors, given in Thomson tetrahedron notation, all lie in the grey (111) plane and are Aδ = ⅙[11$\bar{2}$], δ_B = ⅙[$\bar{1}$2$\bar{1}$], Cδ = ⅙[$\bar{2}$11] and AC = ½[10$\bar{1}$], i.e. consistent with the indexing of Fig. 5. (b) Schematic showing a varying width of the climbed region along the defect, with undulations on the scale of a few nm in a TEM specimen tens of nm in thickness. Large black arrows show the direction of the electron beam, coresponding to Figs. 5 and 6.

results is that the additional layer in most cases is only one atom thick (bearing some resemblance to the formation of interstitial (100) platelets in diamond, which also have only a single additional plane [60]). Certainly atom columns in the climbed fault are not clearly resolved and the ADF-STEM intensity at the fault is lower than adjacent atom columns, which may indicate only partial occupancy. However, this raises the question of what the atomic structure of a monolayer interstitial fault might be, without an obvious answer. A second interpretation is that the extent of climb varies along the dislocation as shown schematically in Fig. 8b. In this case, atom columns would appear blurred and the observed displacement would be some average through the projection of the structure along the electron beam. This is also consistent with the varying displacements that we observe. The varying extent of climb on the defects examined here probably indicates spatial variations in the number of jogs emitting point defects, e.g. due to the difference in density of forest dislocations.

As well as the study of silicon by TD, [45] similar defect microstructures have also been reported in GaAs in the presence of point defect supersaturations [28,61,62]. In all cases climb occurs by absorption of interstitials on 90° partials both in dissociated dislocations and Z-dipoles. Vacancies seem to play little or no part in dislocation climb in these materials, even when plastic deformation produces roughly similar concentrations of vacancies and interstitials. Preferential absorption of interstitials at dislocations has been known for some time (the “dislocation bias” [63]), initially invoked to explain the swelling of irradiated material; vacancies cluster to produce voids, while interstitials are reincorporated in the material at dislocations. Swelling of ion implanted material [64] shows that this mechanism also occurs in diamond. These observations support the idea that, in all materials, vacancies do not become attached to dislocations and instead form clusters. Diamond is perhaps unique only in that the brown coloration that results is visible to the naked eye.

Before discussing our measurement of stacking fault energy, we note that point defect supersaturations induced by plastic deformation have been studied most in ductile fcc metals such as copper and aluminium, [19,65-73] and some quite recent studies have proposed that there is a large imbalance in point defect concentrations, with essentially no interstitials produced by plastic deformation [27,69]. This assertion is based on the lack of a signature for interstitials in materials deformed at very low temperatures, in which point defect migration should be frozen out (e.g. in Cu, $E_i^m \approx 0.1$ eV [66] while $E_v^m \approx 0.7$ eV [70] and vacancy migration occurs at approximately −30 °C). The increase in defect density due to deformation can be detected as an increased electrical resistivity. On heating to room temperature, two signatures of point defect condensation should thus be observed in measurements of resistivity as first interstitials, and then vacancies, become mobile. However, only the higher temperature signal from vacancies is seen [74]. Conversely, irradiation at low temperature produces both signatures upon heating [71,72]. This puzzling result has been confirmed by a battery of other techniques including PAS [73] and Mossbauer spectroscopy [19] (see e.g. reviews [23,27]). Furthermore, TEM studies consistently show a dominance of vacancy dislocation dipoles in deformed material [26]. While we also find a predominance of vacancy dipoles, the evidence here for production of interstitials in deformed diamond is undisputable and it seems most probable that interstitials remain undetected in low-temperature deformed metals due to very low activation energies and pipe diffusion that enables them to be captured on dislocations. Certainly, molecular dynamics simulations of plastic deformation in alloys [75] and metals [76] suggests that chains of interstitials are indeed produced by forest interactions and, at temperatures where interstitials are mobile, these chains break up forming interstitial clusters or small, highly mobile, prismatic dislocation loops [76].

Faulted dipoles are often observed in plastically deformed fcc materials and have been reported in metals (Cu, Ag, Ni, Au) [21,39,40,42,43,77] and semiconductors both with diamond (Si, Ge) [78-82] and zinc-blende structure (GaAs) [28,61,62] so it is not surprising to see them in diamond. In principle, faulted dipoles can occur in two distinct configurations, Z- shape or S- shape, and be either vacancy or interstitial type. In practice however, all observations of faulted dipoles in fcc materials are vacancy type with Z-shape [27,79] and in copper conversion of unfaulted dipoles to faulted ones has been observed in-situ [21]. The absence of interstitial dipoles, which are needed to produce interstitial atoms by the mechanism described in Section 1.1, has been considered by Brown and Nabarro [83,84]. They showed that interstitial dislocation dipoles have a higher energy than vacancy dipoles [85] and proposed mechanisms for one to convert to the other. The ratio of vacancy to interstitial dipoles observed may not, therefore, correspond to the ratio of point defect concentrations.

Since the equilibrium inter-dislocation spacing varies with the dipole height H (Fig. 6d), they have often been used to calculate stacking fault energy [16]. Here, all points in Fig. 7 lie on a single SFE curve, suggesting an equilibrium configuration and that the faulted dipole formed before climb occurred. Our measured SFE of 472 ± 38 mJ m^{-2} is significantly larger than the 279 ± 41 mJ m^{-2} determined by Pirouz et al. [18]. from dissociated 60° dislocations, but similar to their upper limit of 465 mJ m^{-2} determined from faulted dipoles. Since we can simply count the atom spacings, we believe our value to be more reliable. Above a certain height, unfaulted dipoles have a lower energy and the smallest unfaulted dipole separation documented in diamond is 7.4 nm ± 0.8 nm [86]. The largest H we observe for a faulted dipole is 4.73 nm (23 lattice planes), suggesting the transition between unfaulted and faulted configurations occurs between these two values. Dipoles smaller than a critical height H_c are unstable and should collapse to release point defects; Fig. 6a shows that $H_c < 2.47$ nm (12 glide planes).

Overall, our observations of dislocations in brown diamond are consistent with the general understanding of point defect behaviour in other materials with diamond or related structure, and fcc materials in general. Interstitials condense on dislocations, while vacancies form clusters. Some outstanding questions remain, for example why only 90° partials experience climb, and not 30° partials. It would seem that the incorporation of interstitials at the core of a 90° partial dislocation is particularly easy in the diamond structure and since point defects are produced from jogs it may be that pipe diffusion of interstitials along the dislocation line also plays a role. Also, it is not known if these same climbed structures occur more generally in fcc materials; they are perhaps more stable, and therefore have been more readily observed, in materials with diamond structure due to the low mobility of dislocations at room temperature. Finally, the effect of condensed interstitials must play a significant role in work hardening. It has long been appreciated that dislocation dipoles play a central role in this respect, [23] but the detailed mechanism whereby point defects pin dislocations remains to be elucidated.

5. Conclusions

The microstructure of a natural type IIa brown diamond has been examined using different forms of electron microscopy. EBSD, CL, and conventional TEM show clear evidence of plastic deformation, while aberration-corrected ADF-STEM reveals that dissociated dislocations and faulted vacancy dipoles have accreted a significant number of interstitial atoms, resulting in climb of 90° partial dislocations. An interstitial concentration of 10^{17} to 10^{19} cm^{-3} is required to produce the observed microstructure, and calculations show that this could easily be produced by a plastic deformation of ~1% in a diamond that contains pre-existing 'forest' dislocations with a density of 10^7 to 10^9 cm^{-2}. Vacancy clusters are not observed in this study, but vacancy concentrations measured in similar type IIa brown diamonds by PAS ($10^{18}cm^{-3}$) demonstrates that roughly equal concentrations of vacancies and interstitials are produced by plastic deformation.

The observations share common features with previous studies of fcc materials. Interstitials condense on dislocations, while vacancies form clusters. All faulted dipoles were Z-shaped and vacancy type, and the climbed structures appear similar to those seen previously in silicon and GaAs. Climbed regions in many cases appeared to be less than a complete monolayer in thickness, which may indicate partial occupancy or a variable extent of the climbed region along the defect at the nm scale. The faulted dipoles provide a means to measure stacking fault energy, found to be 472 ± 38 mJ m^{-2}.

Author contributions

FHJL performed data acquisition, data analysis, writing – original draft, interpretation of results. RB contributed to data analysis, writing, supervision, interpretation of results. DF contributed to review and editing of manuscript, funding and provided diamond samples. PLD contributed to review & editing of manuscript, suggestion of new experiments and interpretation of results.

Declaration of Competing Interest

The authors declare no completing interests.

Acknowledgements

The authors would like to acknowledge Hugh Leach and John Freeth (De Beers Group Technology), and Jon Newland (Element 6 Ltd) for sample preparation. FHJL acknowledges the EPSRC Centre for Doctoral Training in Diamond Science and Technology (EP/L15315/1) and De Beers Group Technology for funding and loan of natural diamond samples. We thank Ben Breeze and the Spectroscopy RTP at the University of Warwick for their help and use of PL spectrometers. We thank the Warwick Electron Microscopy RTP for use of electron microscopes. We thank Sam Marks and Warwick Manufacturing Group (WMG) for EBSD data collection and equipment use. Additional data related to this publication is available from the University of Warwick data archive at http://wrap.warwick.ac.uk/143532.

Supplementary materials

Supplementary material associated with this article can be found, in the online version, at doi:10.1016/j.actamat.2020.10.033.

References

[1] D. Fisher, S.J. Sibley, C.J. Kelly, Brown colour in natural diamond and interaction between the brown related and other colour-inducing defects, J. Phys.: Condens. Matter 21 (36) (2009).
[2] E.M. Smith, H.H. Helmstaedt, R.L. Flemming, Survival of the brown color in diamond during storage in the subcontinental lithospheric mantle, Canadian Mineralogist 48 (3) (2010) 571–582.
[3] D. Howell, S. Piazolo, D.P. Dobson, I.G. Wood, A.P. Jones, N. Walte, D.J. Frost, D. Fisher, W.L. Griffin, Quantitative characterization of plastic deformation of single diamond crystals: a high pressure high temperature (HPHT) experimental deformation study combined with electron backscatter diffraction (EBSD), Diam. Relat. Mater. 30 (2012) 20–30.
[4] D. Fisher, Brown diamonds and high pressure high temperature treatment, Lithos 112 (2009) 619–624.
[5] V. Avalos, S. Dannefaer, Vacancy-type defects in brown diamonds investigated by positron annihilation, Physica B 340-342 (2003) 76–79.
[6] P. Guagliardo, K. Byrne, J. Chapman, K. Sudarshan, S. Samarin, J. Williams, Positron annihilation and optical studies of natural brown type I diamonds, Diam. Relat. Mater. 37 (2013) 37–40.
[7] J.M. Maki, F. Tuomisto, C.J. Kelly, D. Fisher, P.M. Martineau, Properties of optically active vacancy clusters in type IIa diamond, J. Phys.: Condens. Matter 21 (36) (2009).
[8] L.S. Hounsome, R. Jones, P.M. Martineau, D. Fisher, M.J. Shaw, P.R. Briddon, S. Öberg, Origin of brown coloration in diamond, Phys. Rev. B 73 (12) (2006) 125203.
[9] I.A. Dobrinets, V.G. Nins, Z.A. M., HPHT-Treated Diamonds, Heidelberg, Berlin, 2013.
[10] S. Eaton-Magana, T. Ardon, A.M. Zaitsev, LPHT annealing of brown-to-yellow type Ia diamonds, Diam. Relat. Mater. 77 (2017) 159–170.
[11] B. Willems, P.M. Martineau, D. Fisher, J. Van Royen, G. Van Tendeloo, Dislocation distributions in brown diamond, Physica Status Solidi (a) 203 (12) (2006) 3076–3080.
[12] D. Fisher, D.J.F. Evans, C. Glover, C.J. Kelly, M.J. Sheehy, G.C. Summerton, The vacancy as a probe of the strain in type IIa diamonds, Diam. Relat. Mater. 15 (10) (2006) 1636–1642.
[13] L. Massi, E. Fritsch, A.T. Collins, T. Hainschwang, F. Notari, The "amber centres" and their relation to the brown colour in diamond, Diam. Relat. Mater. 14 (10) (2005) 1623–1629.
[14] U. Bangert, A.J. Harvey, R. Jones, C.J. Fall, A.T. Blumenau, R. Briddon, M. Schreck, F. Hörmann, Dislocation-induced electronic states and point-defect atmospheres evidenced by electron energy loss imaging, New J. Phys. 6 (2004) 184.

[15] U. Bangert, R. Barnes, M.H. Gass, A.L. Bleloch, I.S. Godfrey, Vacancy clusters, dislocations and brown colouration in diamond, J. Phys. Condens. Matter 21 (36) (2009) 364208.
[16] J.W. Steeds, The formation and configurations of faulted dipoles in F.C.C. metals, Philos. Mag.: J. Theoret. Exp. Appl. Phys. 16 (142) (1967) 771–784.
[17] S. Amelinckx, Dislocations in Solids, North-Holland, Amsterdam, 1979, pp. 67–460.
[18] P. Pirouz, D.J.H. Cockayne, N. Sumida, P.B. Hirsch, A.R. Lang, Dissociation of dislocations in diamond, Proc. R. Soc. Lond. A. Math. Phys. Sci. 386 (1791) (1983) 241–249.
[19] A. Seeger, Hyperfine interaction evidence for the existence of two distinct types of self-interstitials in face-centered cubic metals, Phys. Lett. A 89 (5) (1982) 241–244.
[20] J.P. Hirth, On Dislocation Interactions in the fcc Lattice, J. Appl. Phys. 32 (4) (1961) 700–706.
[21] C.B. Carter, The formation and properties of faulted dipoles, Philos. Mag.: J. Theoret. Exp. Appl. Phys. 36 (1) (1977) 147–167.
[22] J. Hornstra, On the type of point defects formed after crossing of dislocations, Acta Metall. 10 (10) (1962) 987–988.
[23] L.M. Brown, Constant intermittent flow of dislocations: central problems in plasticity, Mater. Sci. Technol. 28 (11) (2012) 1209–1232.
[24] A. Seeger, CXXXII. the generation of lattice defects by moving dislocations, and its application to the temperature dependence of the flow-stress of F.C.C. crystals, Lond. Edinburgh Dublin Philos. Mag. J. Sci. 46 (382) (1955) 1194–1217.
[25] L.M. Brown, A dipole model for the cross-slip of screw dislocations in fee metals, Philos. Mag. A 82 (9) (2002) 1691–1711.
[26] M. Niewczas, Transmission electron microscopy observations of debris structure in deformed copper single crystals, Philos. Mag. A 82 (2) (2002) 393–414.
[27] M. Niewczas, Intermittent plastic flow of single crystals: central problems in plasticity: a review, Mater. Sci. Technol. 30 (7) (2014) 739–757.
[28] B.C. De Cooman, C.B. Carter, The formation of faulted dipoles in plastically deformed GaAs, Physica Status Solidi (a) 112 (1) (1989) 41–54.
[29] J.P. Hirth, J. Lothe, Theory of dislocations, Krieger (1991).
[30] B. Slepetz, M. Kertesz, Divacancies in diamond: a stepwise formation mechanism, PCCP 16 (4) (2014) 1515–1521.
[31] J.P. Goss, B.J. Coomer, R. Jones, T.D. Shaw, P.R. Briddon, M. Rayson, S. Oberg, Self-interstitial aggregation in diamond, Phys. Rev. B 63 (19) (2001).
[32] J.P. Goss, B.J. Coomer, R. Jones, C.J. Fall, P.R. Briddon, S. Oberg, Extended defects in diamond: the interstitial platelet, Phys. Rev. B 67 (16) (2003).
[33] M.E. Newton, B.A. Campbell, D.J. Twitchen, J.M. Baker, T.R. Anthony, Recombination-enhanced diffusion of self-interstitial atoms and vacancy-interstitial recombination in diamond, Diam. Relat. Mater. 11 (3–6) (2002) 618–622.
[34] K.Y. Wang, J.W. Steeds, Z.H. Li, H.X. Wang, Annealing and lateral migration of defects in IIa diamond created by near-threshold electron irradiation, Appl. Phys. Lett. 110 (15) (2017).
[35] T. Stachel, J.W. Harris, The origin of cratonic diamonds — constraints from mineral inclusions, Ore Geol. Rev. 34 (1) (2008) 5–32.
[36] J. Ruan, K. Kobashi, W.J. Choyke, On the "'band-A'" emission and boron related luminescence in diamond, Appl. Phys. Lett. 60 (25) (1992) 3138–3140.
[37] D. Takeuchi, H. Watanabe, S. Yamanaka, H. Okushi, H. Sawada, H. Ichinose, T. Sekiguchi, K. Kajimura, Origin of band-A emission in diamond thin films, Phys. Rev. B 63 (24) (2001) 245328.
[38] D. Takeuchi, H. Watanabe, H. Sawada, S. Yamanaka, H. Ichinose, T. Sekiguchi, H. Okushi, Origin of band-A emission in homoepitaxial diamond films, Diam. Relat. Mater. 10 (3) (2001) 526–530.
[39] F. Häussermann, M. Wilkens, Bestimmung der Stapelfehlerenergie kubisch-flächenzentrierter Metalle aus der Analyse des elektronenmikroskopischen Beugungskontrastes von Stapelfehlerdipolen, Physica Status Solidi (b) 18 (2) (1966) 609–624.
[40] C.B. Carter, S.M. Holmes, The study of faulted dipoles in copper using weak-beam electron microscopy, Philos. Mag.: J. Theoret. Exp. Appl. Phys. 32 (3) (1975) 599–614.
[41] M. Sato, Development of faulted dislocation dipoles in silicon during high temperature deformation, Physica Status Solidi (a) 75 (1) (1983) 107–116.
[42] E. Wintner, H.P. Karnthaler, The geometry and formation of faulted dipoles in Cu-Al alloys, Acta Metall. 26 (6) (1978) 941–949.
[43] A. Seeger, G. Wobser, Stapelfehlerdipole in kubisch-flächenzentrierten Metallen, Physica Status Solidi (b) 18 (1) (1966) 189–206.
[44] M.H. Grimsditch, A.K. Ramdas, Brillouin scattering in diamond, Phys. Rev. B 11 (8) (1975) 3139–3148.
[45] J. Thibault-Desseaux, H.O.K. Kirchner, J.L. Putaux, Climb of dissociated dislocations in silicon, Philos. Mag. A 60 (3) (1989) 385–400.
[46] D. Cherns, G. Feuillet, The mechanism of dislocation climb in GaAs under electron irradiation, Philos. Mag. A 51 (5) (1985) 661–674.
[47] A. Pu, T. Bretagnon, D. Kerr, S. Dannefaer, Positron annihilation investigation of vacancies in as-grown and electron-irradiated diamonds, Diam. Relat. Mater. 9 (8) (2000) 1450–1463.
[48] C.M. Breeding, S. Eaton-Magana, J.E. Shigley, Natural-color green diamonds: a beautiful conundrum, Gems Gemol. 54 (1) (2018) 2–27.
[49] S. Eaton-Magaña, Comparison of luminescence lifetimes from natural and laboratory irradiated diamonds, Diam. Relat. Mater. 58 (2015) 94–102.
[50] J. Koike, D.M. Parkin, T.E. Mitchell, Displacement threshold energy for type IIa diamond, Appl. Phys. Lett. 60 (12) (1992) 1450–1452.
[51] J.W. Steeds, S. Kohn, Annealing of electron radiation damage in a wide range of Ib and IIa diamond samples, Diam. Relat. Mater. 50 (2014) 110–122.
[52] L. Speich, S.C. Kohn, G.P. Bulanova, C.B. Smith, The behaviour of platelets in natural diamonds and the development of a new mantle thermometer, Contrib. Mineral. Petrol. 173 (5) (2018) 39.
[53] G.S. Woods, F.C. Frank, Platelets and the infrared absorption of type Ia diamonds, Philos. Mag.: J. Theoret. Exp. Appl. Phys. 407 (1832) (1986) 219–238.
[54] E.J. Brookes, P. Greenwood, G. Xing, The plastic deformation and strain-induced fracture of natural and synthetic diamond, Diam. Relat. Mater. 8 (8–9) (1999) 1536–1539.
[55] H. Bracht, J.F. Pedersen, N. Zangenberg, A.N. Larsen, E.E. Haller, G. Lulli, M. Posselt, Radiation enhanced silicon self-diffusion and the silicon vacancy at high temperatures, Phys. Rev. Lett. 91 (24) (2003) 245502.
[56] Y. Shimizu, M. Uematsu, K.M. Itoh, Experimental evidence of the vacancy-mediated silicon self-diffusion in single-crystalline silicon, Phys. Rev. Lett. 98 (9) (2007) 095901.
[57] H. Bracht, N.A. Stolwijk, H. Mehrer, Properties of intrinsic point defects in silicon determined by zinc diffusion experiments under nonequilibrium conditions, Phys. Rev. B 52 (23) (1995) 16542–16560.
[58] B. Décamps, D. Cherns, M. Condat, The climb of dissociated dislocations in a quenched Cu-13•43 at.% Al alloy, Philos. Mag. A 48 (1) (1983) 123–137.
[59] D. Cherns, P.B. Hirsch, H. Saka, Mechanism of climb of dissociated dislocations, Philos. Mag.: J. Theoret. Exp. Appl. Phys. 371 (1745) (1980) 213–234.
[60] D. Cherns, K. Kaneko, A. Hovsepian, A. Lang, Measurement of the lattice displacement across {100} platelets in diamond by large-angle convergent-beam electron diffraction, Philos. Mag. A 75 (6) (1997) 1553–1566.
[61] I. Yonenaga, S.-.H. Lim, D. Shindo, P.D. Brown, C.J. Humphreys, Structure and climb of faulted dipoles in GaAs, Physica Status Solidi (a) 171 (1) (1999) 53–57.
[62] S.H. Lim, D. Shindo, I. Yonenaga, P.D. Brown, C.J. Humphreys, Atomic arrangement of a Z-Shape faulted dipole within deformed GaAs, Phys. Rev. Lett. 81 (24) (1998) 5350–5353.
[63] P.T. Heald, The preferential trapping of interstitials at dislocations, Philos. Mag.: J. Theoret. Exp. Appl. Phys. 31 (3) (1975) 551–558.
[64] J.F. Prins, T.E. Derry, J.P.F. Sellschop, Volume expansion of diamond during ion implantation, Phys. Rev. B 34 (12) (1986) 8870–8874.
[65] T. Blewitt, R. Coltman, J. Redman, Defects in crystalline solids, Phys. Soc. London (1955).
[66] M. Niewczas, Z.S. Basinski, J.D. Embury, Deformation of copper single crystals to large strains at 4.2K, Philos. Mag. A 81 (5) (2001) 1143–1159.
[67] M. Niewczas, Z.S. Basinski, S.J. Basinski, J.D. Embury, Deformation of copper single crystals to large strains at 4.2K, Philos. Mag. A 81 (5) (2001) 1121–1142.
[68] Z.S. Basinski, S.J. Basinski, Electrical resistivity of fatigued copper crystals, Acta Metall. 37 (12) (1989) 3275–3281.
[69] S. Saimoto, M. Niewczas, M.R. Langille, B. Diak, Specific resistivity of dislocations and vacancies for super-pure aluminium at 4.2 K determined in-situ and post-recovery deformation and correlated to flow stress, Philos. Mag. 99 (22) (2019) 2770–2788.
[70] R.R. Bourassa, B. Lengeler, The formation and migration energies of vacancies in quenched copper, J. Phys. F Met. Phys. 6 (8) (1976) 1405–1413.
[71] W. Mansel, G. Vogl, Fast-neutron radiation-damage in aluminium studied by interstitial trapping at Co-57 Mossbauer atoms, J. Phys. F-Metal Phys. 7 (2) (1977) 253–271.
[72] D.W. Keefer, J.C. Robinson, A. Sosin, Modulus effects in metals after low temperature electron irradiation—III. aluminum, Acta Metall. 16 (7) (1968) 927–937.
[73] C. Dauwe, M. Dorikens, L. Dorikens-Vanpraet, D. Segers, Positron lifetimes and lineshape factors in deformed copper, Appl. Phys. A 5 (2) (1974) 117–120.
[74] H. Kressel, N. Brown, Lattice defects in shock-deformed and cold-worked nickel, J. Appl. Phys. 38 (4) (1967) 1618–1625.
[75] D.S. Xu, H. Wang, R. Yang, P. Veyssiere, Point Defect Formation By Dislocation Reactions in TiAl, in: W. Cai, K. Edagawa, A.H.W. Ngan (Eds.), Dislocations 20082009.
[76] H. Wang, D.S. Xu, P. Veyssiere, R. Yang, Interstitial loop strengthening upon deformation in aluminum via molecular dynamics simulations, Acta Mater. 61 (9) (2013) 3499–3508.
[77] Z. Yan, Y. Lin, Faulted dipoles in a nanostructured 7075 Al alloy produced via high-pressure torsion, Mater. Sci. Eng.: A 754 (2019) 232–237.
[78] A.T. Winter, S. Mahajan, D. Brasen, Weak-beam electron microscopy of faulted dipoles in deformed silicon, Philos. Mag. A 37 (3) (1978) 315–326.
[79] S.W. Chiang, C.B. Carter, D.L. Kohlstedt, Faulted dipoles in germanium a high--resolution transmission electron microscopy study, Philos. Mag. A 42 (1) (1980) 103–121.
[80] J.C.H. Spence, H. Kolar, Lattice imaging of faulted dipoles in silicon, Philos. Mag. A 39 (1) (1979) 59–63.
[81] Y. Nishino, T. Imura, Dislocation configurations induced by cyclic deformation in silicon crystals, Physica Status Solidi (a) 78 (2) (1983) 655–663.
[82] Y. Nishino, H. Saka, T. Imura, Dislocation configurations characteristic of deformed czochralski-grown silicon crystals, Physica Status Solidi (a) 70 (2) (1982) 729–737.
[83] L.M. Brown, F.R.N. Nabarro, The enumeration and transformation of dislocation dipoles II. the transformation of interstitial dipoles into vacancy dipoles in an open dislocation array, Philos. Mag. 84 (3–5) (2004) 441–450.
[84] F.R.N. Nabarro, L.M. Brown, The enumeration and transformation of dislocation dipoles I. the dipole strengths of closed and open dislocation arrays, Philos. Mag. 84 (3–5) (2004) 429–439.
[85] J.G. Antonopoulos, L.M. Brown, A.T. Winter, Vacancy dipoles in fatigued copper, Philos. Mag.: J. Theoret. Exp. Appl. Phys. 34 (4) (1976) 549–563.
[86] A. Mussi, D. Eyidi, A. Shiryaev, J. Rabier, TEM observations of dislocations in plastically deformed diamond, Physica Status Solidi (a) 210 (1) (2013) 191–194.